Available online at website: https://journal.bcrec.id/index.php/bcrec

Bulletin of Chemical Reaction Engineering & Catalysis, 20 (3) 2025, 392-402

Original Research Article

One-step Hydrothermal Synthesis of Fe_3O_4/GO Composites Combined with Persulfate for the Removal of Reactive Black in Aqueous Solution

Zhaonan Sun[1], Wei Zhao[1], Jiayi Wu[1], Ke Shi[2,3], Lin Zhang[1], Wei Kou[1*]

[1]Liaoning Key Laboratory of Chemical Additive Synthesis and Separation Project, Yingkou Institute of Technology, Yingkou 115014, China.
[2]Key Laboratory of Pollution Ecology and Environmental Engineering, Shenyang Institute of Applied Ecology, China Academy of Sciences, Shenyang 110016, China
[3]University of Chinese Academy of Sciences, Beijing 10049, China

Received: 14th February 2025; Revised: 7th May 2025; Accepted: 8th May 2025
Available online: 14th May 2025; Published regularly: October 2025

Abstract

An environmentally friendly magnetic Fe_3O_4/graphene oxide (Fe-GO) composite was synthesized via a hydrothermal method for persulfate (PDS) activation. The composite was systematically characterized using Scanning Electron Microscopy (SEM), Energy-Dispersive X-ray Spectroscopy (EDS), and Brunauer-Emmett-Teller (BET) analysis. Furthermore, the degradation performance of reactive black 5 (RB5) in the composite/PDS system was investigated under varying conditions, including composite dosage, PDS concentration, initial RB5 concentration, solution pH, and oscillation frequency. The experiments showed that the RB5 removal efficiency could reach 99.2% with good reproducibility under the conditions of 0.8 g/L of composites, 3 mol/L of PDS, 200 r/min of stirring speed, pH ≈ 6, and 25 ℃ for 180 min. Quenching experiments showed that four active reactive substances, sulfate radicals (SO_4^{-}·), hydroxyl radicals (·OH), oxygen radicals (O_2^{-}) and single linear oxygen ($^1O_2$), existed in the composite/PDS system, of which $^1O_2$ played a crucial role in the degradation of RB5. Cycling tests showed that the Fe-GO composites were stable and had good application prospects.

Keywords: Fe_3O_4; Graphene; Graphene Oxide; Persulfate; Hydrothermal Method; Dyes

How to Cite: Sun, Z., Zhao, W., Wu, J., Shi, K., Zhang, L., Kou, W. (2025). One-step Hydrothermal Synthesis of Fe_3O_4/GO Composites Combined with Persulfate for the Removal of Reactive Black in Aqueous Solution. *Bulletin of Chemical Reaction Engineering & Catalysis*, 20 (3), 392-402. (doi: 10.9767/bcrec.20355)

Permalink/DOI: https://doi.org/10.9767/bcrec.20355

1. Introduction

With the rapid development of the dye production and printing and dyeing industries, the discharge volume of dye wastewater containing large amounts of sizing agents, dyes, auxiliaries, surfactants and other components has increased dramatically [1,2]. Studies have shown that most dye molecules are teratogenic, carcinogenic and mutagenic. Moreover, due to their complex structures, most dyes exhibit strong resistance to degradation [3,4]. Among them, Reactive Black 5 (RB5), a typical azo dye, is widely used in the printing and dyeing industry. However, its wastewater is characterized by high chemical oxygen demand (COD), strong chromaticity, and poor biodegradability, making it a challenging issue in treatment [5,6]. Therefore, there is an urgent need for an economical and efficient treatment technology to minimize its impact on the ecosystem.

The commonly used treatment methods at present include adsorption methods [7,8], coagulation methods [9], biological methods [10], advanced oxidation methods, etc. [11,12] Advanced Oxidation Processes (AOPs), based on

* Corresponding Author.
Email: kouwei6@126.com (W.Kou)

sulfate radicals ($SO_4^{\cdot-}$), have received extensive attention from researchers due to their ability to effectively degrade recalcitrant organic pollutants [13,14]. Compared with hydroxyl radicals (·OH), $SO_4^{\cdot-}$ possesses a higher redox potential and stronger oxidizing ability, a relatively wide pH range (2-11), and a longer half-life, enabling it to eliminate most refractory organic pollutants. Consequently, $SO_4^{\cdot-}$ exhibits significant advantages in the degradation or mineralization of both traditional and emerging pollutants [15,16]. The $SO_4^{\cdot-}$ can be generated by activating persulfate through methods such as heat, alkalinity, radiation (ultraviolet light, ultraviolet light, ultrasound, gamma rays), transition metals [17] and carbon-based materials [18]. Among them, transition metals (especially iron), with the characteristics of simple activation, high cost-effectiveness, and being relatively environmentally friendly, have become persulfate activators [19], such as: Fe^0, Fe_2O_3, FeOOH and Fe_3O_4. However, due to its strong magnetism and large surface energy, Fe_3O_4 is prone to aggregation in the liquid phase, which reduces its activation ability [20], and restricts its application to some extent. Some studies have attempted to prepare composite materials by combining materials such as carbon nanotubes, graphene, and biochar (BC) with Fe_3O_4 to improve the dispersibility of Fe_3O_4 in the liquid phase [21,22]. Therefore, in recent years, Fe_3O_4/graphene oxide (GO) magnetic nanocomposites have attracted widespread attention regarding their activation and adsorption properties [23]. Yasamansadat *et al*. [24] utilized graphene oxide/Fe_3O_4 for the adsorption and removal of methyl tert-butyl ether, achieving a maximum adsorption capacity of up to 399 mg/g. Wang *et al*. [25] first reported the in situ preparation of nitrogen-doped graphene oxide-supported nano-Fe_3O_4 (Fe_3O_4@NRGO-10) by using ionizing radiation. It was found that it exhibited excellent catalytic activity for activating peroxymonosulfate to degrade phenol, sulfamethoxazole, bisphenol A, and atrazine, with wide applicability.

However, previous studies have demonstrated the potential of transition metal/carbon matrix composites in the activation of persulfate for the degradation of organic pollutants. However, there are still limitations, such as long preparation period and weak interfacial bonding due to the multi-step composite process for the synthesis of materials, as well as the susceptibility of traditional transition metal catalysts to secondary contamination due to metal leaching and poor cycling stability. The hydrothermal method is a simple yet powerful technique for growing crystalline materials without the need for surfactants. It significantly minimizes reaction time and energy consumption, while allowing precise control over the size and shape of synthesized products through adjustments in reaction parameters [26,27]. In view of this, the Fe_3O_4/graphene oxide composite (hereinafter referred to as Fe-GO) was prepared in one step by the hydrothermal method. Taking RB5 as the target pollutant, the efficacy and mechanism of the Fe-GO-activated persulfate system in degrading dye wastewater were explored, aiming to find a persulfate activator with good activation effect and simple preparation method, thereby providing a theoretical basis for its engineering application.

2. Materials and Methods

2.1 Materials

Graphene oxide (⩾99%) was sourced from Shenzhen Suiheng Technology Co., Ltd. Reactive Black 5 (⩾99%), potassium bromide, p-benzoquinone, and L-histidine were obtained from Shanghai Macklin Biochemical Co., Ltd. Sodium persulfate, methanol, tert-butanol, and phenol were from Tianjin Damao Chemical Reagent Factory. Anhydrous ethanol was supplied by Tianjin Fuyu Fine Chemicals Co., Ltd. Ammonia water was from Tianjin Kermel Chemical Reagent Co., Ltd. Ferric chloride was sourced from Tianjin Beilian Fine Chemicals Development Co., Ltd. Ferrous sulfate and sodium hydroxide were from Tianjin Zhiyuan Chemical Reagent Co., Ltd., and sulfuric acid was from Kunshan Jincheng Reagent Co., Ltd. All the reagents used in the experiment were of analytical grade.

2.2 Materials Preparation

Fe-GO was prepared by the hydrothermal method. Firstly, 0.16 g of graphene oxide powder, 1.0 g of $FeSO_4{\cdot}7H_2O$, and 1.9 g of $FeCl_3{\cdot}6H_2O$ were weighed and added into 100 mL of deionized water. After being stirred in a water bath at 95 °C for 60 min, pH was adjusted to 11. The heating was then stopped, and after cooling to 25 °C, the prepared Fe_3O_4/graphene composite was centrifuged (8000 r/min) for 20 min using a high-speed centrifuge (TG16-WS). It was washed with distilled water until neutral, and then freeze-dried at -20 °C for no less than 72 h. Finally, it was sealed and placed in a desiccator for later use.

2.3 Materials Characterizations

The surface structures of GO and Fe-GO were characterized and analyzed using SEM (Regulus 8100). Paired with EDS (Oxford ULTIM MAX 40), the distribution of Fe elements on their surfaces was semi-quantitatively analyzed through elemental image distribution to investigate the Fe loading situation on the graphene oxide surface.

The specific surface area, porosity, and pore size of the composite material were determined by BET (ASAP 2460 3.01). The crystal structures of GO and Fe-GO were detected using XRD (D8advance) to examine the Fe_3O_4 loading on the graphene oxide surface. In the experiment, Cu-Kα radiation was used as the radiation source, with a scanning range of 10 - 80°, a voltage of 40 kV, and a current of 20 mA. The magnetism of the prepared Fe-GO was analyzed using a vibrating sample magnetometer (JDAW-2000D) to investigate its recyclability.

2.4 Experimental Procedures

All experiments were conducted in 150 mL Erlenmeyer flasks at an ambient temperature of 25 °C. The efficacy and influencing factors of the Fe-GO-activated persulfate (PDS) prepared in 2.2 were investigated using the single-factor method. Firstly, 0.05 g of Fe-GO was added to 100 mL of simulated RB5 dye wastewater with a concentration of 50 mg/L. The reaction was carried out under the conditions of a temperature of 25 °C, a PDS dosage of 1 mmol/L, an oscillation frequency of 200 r/min, and a pH value of 6. The Erlenmeyer flasks were placed in a constant-temperature oscillator, and samples were taken at different time points (15, 30, 60, 90, 120, 180 min). The absorbance values of the effluent were measured at λ600 nm using ultraviolet-visible spectrophotometry (UV-S800PC). The effluent concentration (C_1) was calculated according to the concentration-absorbance standard curve (y = 0.021x + 0.02, R^2 = 0.997). The active efficacy of the Fe-GO composite was evaluated and the optimal activation conditions were determined by comparing C_1/C_0.

3 Results and Discussion

3.1 Characterization of Fe-GO

Figure 1 presented the characteristic surface morphology and elemental composition of GO and Fe-GO as revealed by SEM and EDS. The comparative SEM analysis in Figure 1(a)-(b) demonstrated that the Fe-GO composite exhibited a rougher surface morphology with distinct granular features compared to pristine GO. This structural modification effectively enhances the interlayer spacing of the material, thereby suppressing the stacking aggregation commonly observed in unmodified graphene oxide. Furthermore, EDS elemental mapping provides direct evidence of successful iron incorporation. As shown in Figure 1(c)-(f), the iron content increased remarkably from 0.8 wt% in GO to 37.8 wt% in Fe-GO, with homogeneous spatial distribution of Fe elements across the modified material surface. These quantitative results confirm the effectiveness of the hydrothermal synthesis method in achieving covalent bonding between iron species and oxygen-containing functional groups on the graphene oxide matrix. The successful magnetic modification was further corroborated by subsequent magnetization measurements.

Figure 2 showed the XRD, VSM, and BET graphs of GO and Fe-GO. By comparing and

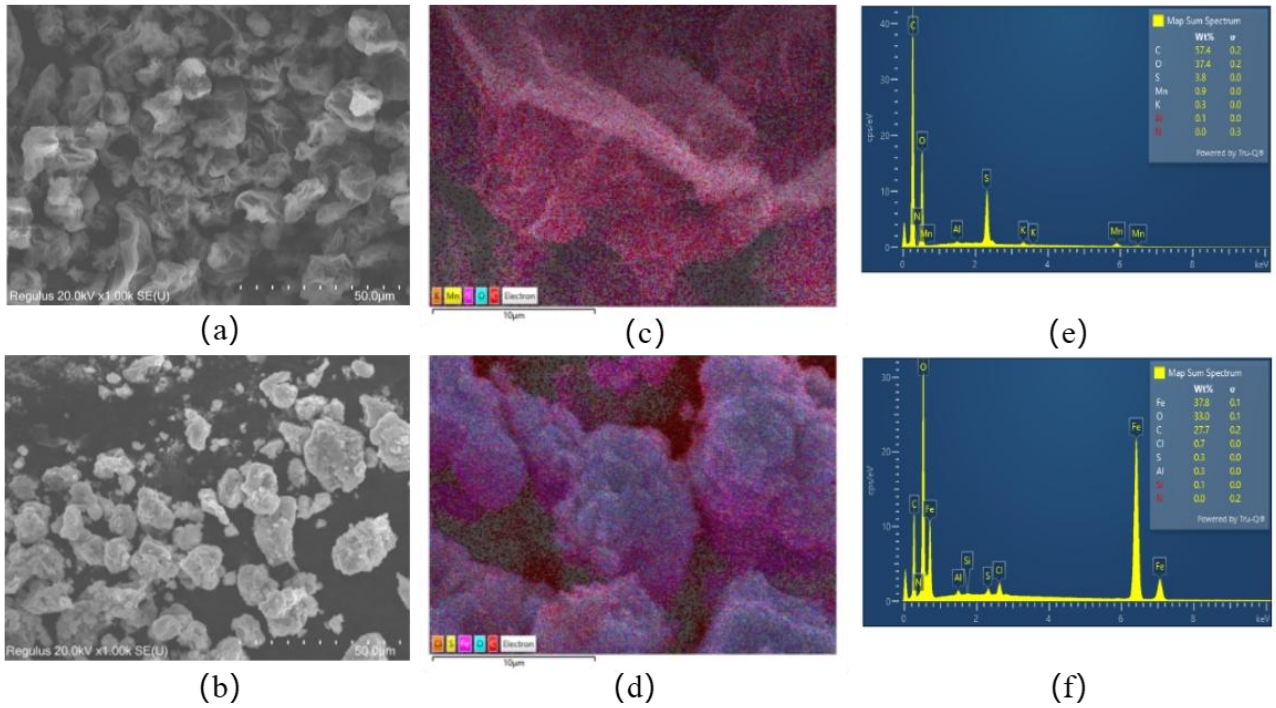

Figure 1. SEM and EDS of GO and Fe-GO: (a) SEM image of GO; (b) SEM image of Fe-GO; (c) and (e) EDS spectrum of GO; (d) and (f) EDS spectrum of Fe-GO.

analyzing the GO and Fe_3O_4 standard cards in Figure 2(a), it could be seen that the diffraction peaks of Fe_3O_4 appear in Fe-GO, and there were no obvious impurity phase peaks. The diffraction peaks of Fe-GO at 2θ angles of 30.1°, 35.5°, 37.1°, 57.0°, and 62.6° correspond to the (220), (311), (222), (511), and (440) crystal planes of Fe_3O_4 respectively, indicating the existence of face-centered cubic crystal structure of Fe_3O_4, which demonstrated that Fe_3O_4 has been successfully loaded on the surface of graphene oxide materials by the hydrothermal method [28]. As could be seen from the VSM results of Fe-GO (Figure 2(b)), the hysteresis loop of Fe-GO was of a typical S-shape. In the absence of a driving force, the remanent magnetization was close to zero, with no coercivity and remanence. Therefore, it indicated that the prepared Fe-GO composite was a superparamagnetic material [29].

Through an external magnetic field, the rapid separation of Fe-GO from the aqueous solution could be achieved efficiently, that was, it exhibited good magnetic separation performance compared with GO. As shown in Figure 2(c), the N_2 adsorption-desorption isotherm curve of Fe-GO belonged to Type IV. The hysteresis loop could serve as one of the bases for judging the width of the pore size distribution. The existence of the hysteresis loop implied the presence of a mesoporous structure, which was consistent with the research findings of Li *et al.* [30]. The BET results revealed that the specific surface area of GO was 6.70 m^2/g. While the specific surface area of Fe-GO was 73.2377 m^2/g, with an average pore diameter of 15.926 nm, indicating it was mesoporous. The relatively large specific surface area was conducive to providing adsorption sites and activation sites, thereby enhancing the adsorption and activation capabilities of the material. After the activation reaction, the specific surface area of Fe-GO was 77.6362 m^2/g, with an average pore diameter of 13.8377 nm, and the

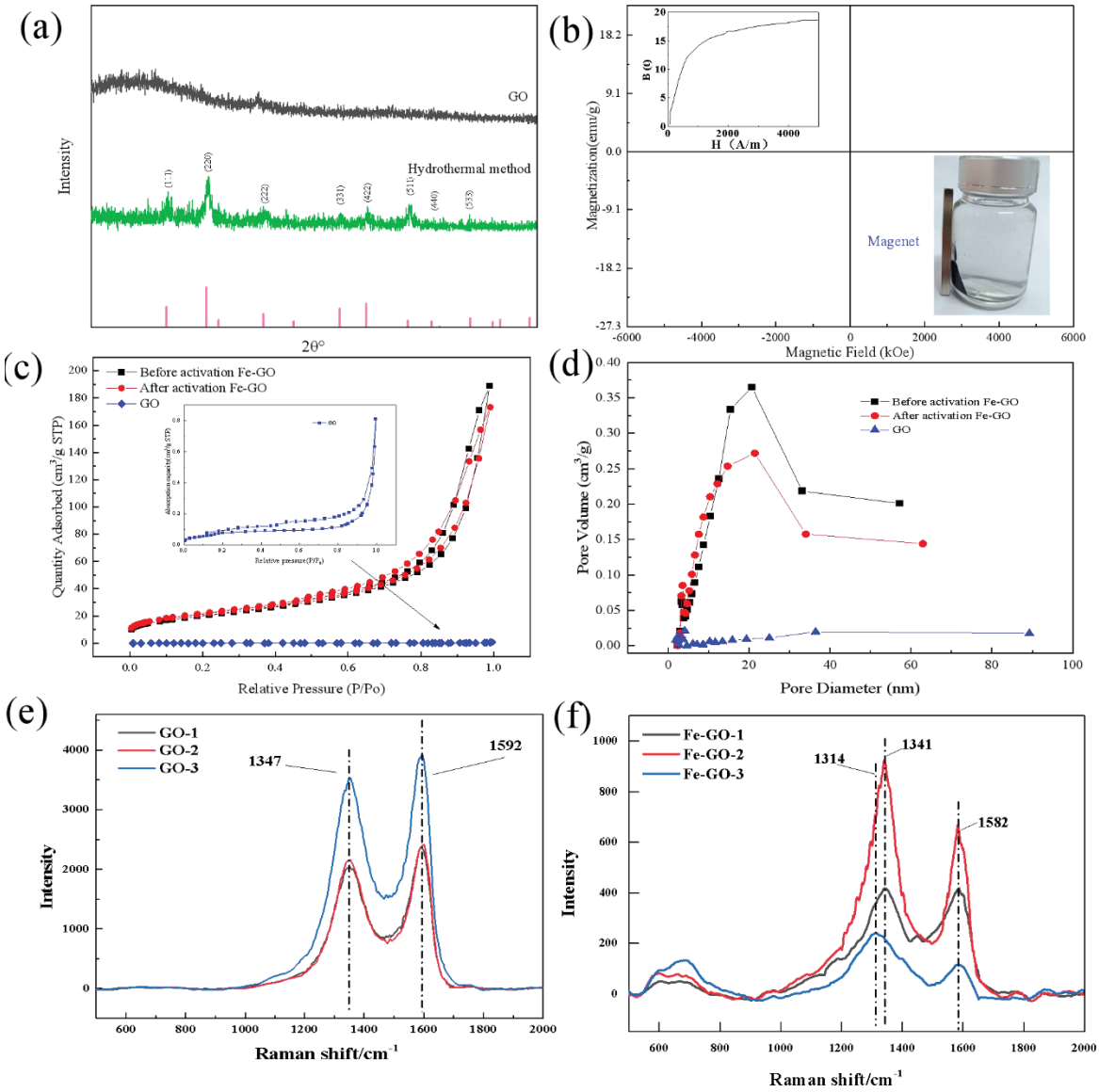

Figure 2. Characterizations of Fe-GO and GO (a) XRD (b) VSM (c) N_2 adsorption-desorption isotherm curve (d) Pore volume (e) and (f) Raman of GO and Fe-GO.

mesopore distribution was more uniform. To a certain extent, this suggested that during the activation process, the adsorption sites provided by Fe-GO for RB5 were removed due to activation, laying the foundation for the recycled use of Fe-GO.

Figure 2(e)-(f) displayed the comparative Raman spectroscopic analysis of graphene oxide (GO) and its iron-modified counterpart (Fe-GO), providing critical insights into their structural defects and graphitic ordering. Both materials exhibited characteristic carbon vibrational modes: the disorder-induced *D* band at 1350 cm^{-1} and the graphitic G band at 1580 cm^{-1}. The intensity ratio (I_D/I_G) served as a quantitative indicator of structural defects, where increased values correspond to higher defect density and lower graphitic crystallinity. Notably, the Fe-GO composite demonstrated a substantial enhancement in defect density, as evidenced by the I_D/I_G ratio increasing from 0.882 in pristine GO to 1.29 after iron modification (46.1% increase).

3.2 The Performance of Activating PDS to Degrade RB5 in Different Systems

Figure 3 illustrated the effects of the systems GO/PDS, PDS, and Fe-GO/PDS to degrade RB5. The analysis showed that with the prolongation of the reaction time, the effluent concentration of RB5 in the GO/PDS system slightly decreased first and then levels off. In contrast, in the Fe-GO/PDS system, the effluent concentration of RB5 rapidly decreased within the first 10 min and then slows down but still maintained a downward trend. After 180 min of reaction, the removal rates of RB5 in the GO/PDS, PDS and Fe-GO/PDS systems were 10%, 12% and 76% respectively. That is, the degradation effect of the Fe-GO/PDS system on RB5 was significantly improved compared with that of the GO/PDS system, indicating that the adsorption and activation properties of Fe-GO were obviously superior to those of GO, which was consistent with the characterization results in Section 3.1. Therefore, the Fe-GO/PDS system was selected as the subject for subsequent research, and its influencing factors will be optimized.

3.3 Study on the Influencing Factors of the Degradation of RB5 in the GO/PDS System

3.3.1 The influence of the dosage of PDS

For the treatment of RB5 dye wastewater by the Fe-GO/PDS system, the dosage of PDS directly affected the generation amount of radicals such as $SO_4^{-\cdot}$ in the reaction system, thereby influencing the removal effect. Figure 4 showed the impact of the PDS dosage on the removal effect of RB5 degradation in the Fe-GO/PDS system. The analysis revealed that under different dosages of PDS, with the increase of reaction time, the removal efficiency of RB5 by Fe-GO was continuously enhanced. Increasing the PDS dosage leads to a significant improvement in the removal efficiency of RB5. When the PDS dosage was 0 mmol/L, the removal rate of RB5 by Fe-GO was 35.0%, indicating its certain adsorption capacity; when the dosage was 4 mmol/L, the removal rate of RB5 reached 99.9%. When the dosages were 3 mmol/L and 4 mmol/L, the removal effects on RB5 were similar. In the initial stage, excessive PDS scavenged $SO_4^{-\cdot}$ and ·OH radicals by generating peroxydisulfate radicals ($S_2O_8^{2-}$), resulting in an insignificant improvement in the removal effect. This research finding was consistent with that of Xiao *et al.* [31]. Taking all factors into consideration, 3 mmol/L was determined as the appropriate dosage of PDS and was used for subsequent research.

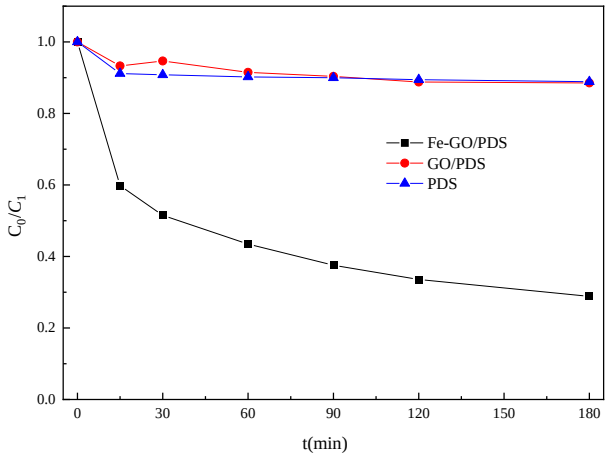

Figure 3. Degradation of RB5 by PDS activated by GO and Fe-GO (conditions: [Fe-GO] or [GO] = 0.05 g, [PDS] = 1 mmol/L, T = 25 ℃, v = 200 r/min, pH_0 ≈ 6, [RB5] = 50 mg/L, and t = 180 min.)

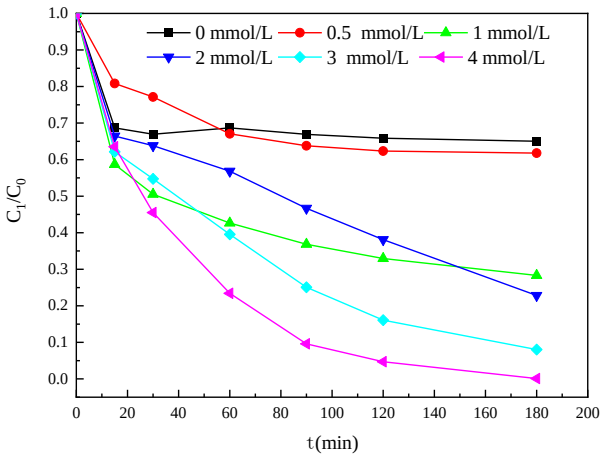

Figure 4. Effect of PDS dosage on RB5 removal efficiency (conditions: [Fe-GO] = 0.05 g, T = 25 ℃, v = 200 r/min, pH_0 ≈6, [RB5] = 50 mg/L, and t = 180 min.).

3.3.2 The influence of the dosage of Fe-GO

The dosage of the catalyst can affect the process of peroxisulfate being activated to generate radicals under the action of the catalyst, and it is also closely related to the cost of water treatment [32]. Given that Fe-GO itself possessed certain adsorption capabilities and adsorption might occur during the reaction process, the activation and adsorption of Fe-GO were simultaneously investigated. Figure 5 showed the impact of the dosage of Fe-GO on the removal efficiency of RB5 in the Fe-GO/PDS activation system and the Fe-GO adsorption system. As could be seen from Figure 5(a), for different dosages of Fe-GO, the effluent concentration of RB5 in the Fe-GO adsorption system first decreased and then tended to level off. However, the higher the dosage of Fe-GO, the lower the effluent concentration of RB5. After a reaction time of 180 min, the maximum removal rate of RB5 could reach 59.8%, indicating that Fe-GO had a certain adsorption effect on RB5. Analysis of Figure 5(b) revealed that the effluent concentration of RB5 continuously decreased with the increase in reaction time. After a reaction time of 180 min, the maximum removal rate of RB5 by Fe-GO could reach 93.9%. Within the range of 0.2 g/L to 0.8 g/L, the higher the dosage of Fe-GO, the faster the effluent concentration of RB5 decreased. When the dosage of Fe-GO increased from 0.8 g/L to 1 g/L, the change trend of the removal rate of RB5 was approximately the same without significant improvement. Comprehensive analysis showed that the higher the dosage of Fe-GO, the more activation sites and adsorption sites were provided, resulting in a better removal effect of RB5. However, for wastewater with a given concentration, an excessive dosage of Fe-GO not only failed to significantly improve the degradation effect but also caused a waste of reagents. It could be seen that an appropriate reagent dosage was of great significance for both the degradation effect and cost. Therefore, in this study, a suitable dosage of Fe-GO, 0.8 g/L, was determined and used for subsequent research. Meanwhile, comparative analysis indicated that the degradation effect of RB5 in the Fe-GO/PDS activation system was significantly better than that in the Fe-GO adsorption system, demonstrating that Fe-GO had good activation performance and that the removal of RB5 was the result of the synergistic effect of the adsorption of Fe-GO and the activation of PDS.

3.3.3 The influence of oscillation frequency

An appropriate oscillation frequency is conducive to enhancing the mass transfer process in the Fe-GO/PDS/RB5 system. A proper increase in the oscillation frequency can boost the mass transfer rate of RB5 in the solution, enabling it to quickly reach the surface of Fe-GO. Meanwhile, it also augments the collision opportunities among RB5, Fe-GO, and $SO_4^{\cdot-}$, thereby enhancing the degradation rate of RB5. Figure 6 illustrated the impact of the oscillation frequency on the removal efficiency of RB5 in the Fe-GO/PDS system. As could be seen from the figure, when the oscillation frequency increased from 150 r/min to 250 r/min, the removal rate of RB5 first rised rapidly and then tended to level off. Moreover, the higher the oscillation frequency, the faster the degradation rate of RB5. After a reaction time of 180 min, the removal rate of RB5 could reach over 94%. However, a relatively large oscillation frequency (250 r/min) did not significantly improve the removal effect of RB5. On the contrary, considering comprehensively, a moderate oscillation frequency (200 r/min) is selected for subsequent research.

3.3.4 The impacts of initial dye concentration

Under normal circumstances, for a given Fe-GO/PDS system, the higher the pollutant

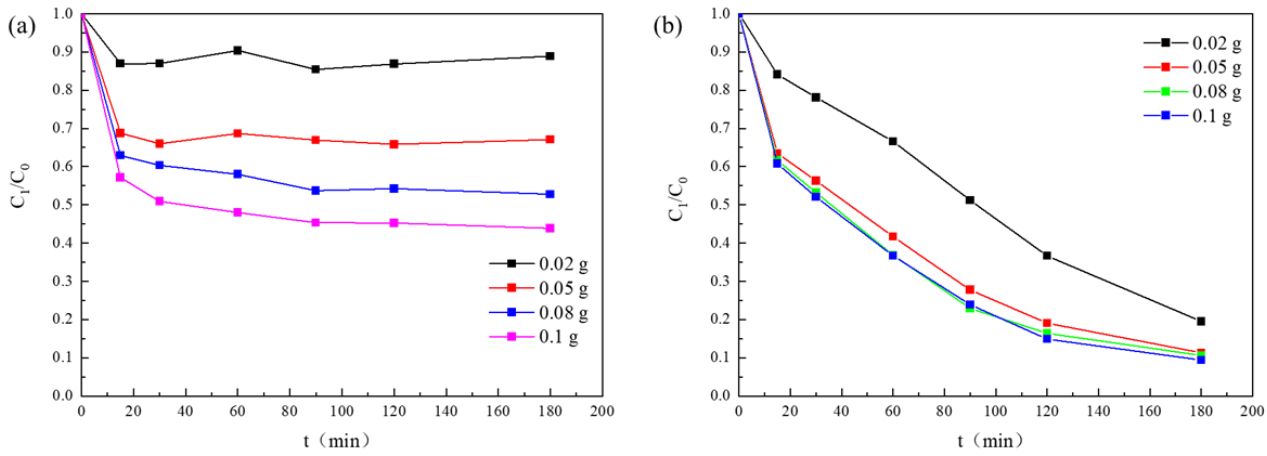

Figure 5. Effect of Fe-GO dosage on RB5 removal: (a) Fe-GO adsorption system (b) Fe-GO/PDS activation system (conditions:[PDS] = 3 mmol/L, T = 25 ℃, v = 200 r/min, pH_0 ≈6, [RB5] = 50 mg/L, and t = 180 min)

concentration, the poorer the treatment effect. Figure 7 showed the impact of the initial concentration of RB5 on the removal efficiency of RB5 in the Fe-GO/PDS system. Overall, the removal rate of RB5 increased with the increase in reaction time. When the initial concentration was relatively low (20 mg/L), the effluent concentration of RB5 in the activation system rapidly decreased and then tended to stabilize, with the removal rate of RB5 approaching 100%, mainly because RB5 was completely degraded within a short period of time. As the initial concentration of RB5 gradually increased (from 50 mg/L to 200 mg/L), the effluent concentration of RB5 becomed higher and the reaction rate gradually decreased. The analysis revealed that under the condition of constant dosages of Fe-GO and PDS, the number of adsorption and activation sites provided was fixed, and the amount of radicals generated was limited, that is, the amount of degradable organic matter was limited. The experimental results showed that the best treatment effect was achieved when the initial concentration of RB5 was 20 mg/L. And as the initial concentration of RB5 increases, the effluent water quality becomed worse.

3.3.5 The impacts of initial pH

Some studies have shown [33] that a series of factors such as the charges on the catalyst surface, the degree of ionization of peroxydisulfate (PS), the target pollutants to be treated, and the transformation of free radicals can all affect the degradation efficiency of the catalyst. The change in the acidity and alkalinity of the solution can also alter the catalytic performance of the catalyst. During the oxidation process of peroxydisulfate, it is mainly the free radicals, such as $SO_4^{-\cdot}$ that act on the target pollutants to remove them, and the pH value of the solution, can affect the activity of free radicals, thereby exerting an impact on the degradation of RB5 by the Fe-GO/PDS activation system. Figure 8 showed the impact of the initial pH on the removal efficiency of RB5 in the Fe-GO/PDS system. As could be seen from the figure, for different initial pH values, the removal rate of RB5 increased with the increase in time. The lower the pH value, the stronger the acidity, and the faster the reaction rate. This phenomenon can be attributed to the superior catalytic activity of Fe-GO under acidic conditions. In contrast, alkaline conditions induce modifications in the surface properties of carbon materials, promoting the formation of oxygen-containing functional groups and consequently diminishing catalytic performance [34]. Furthermore, $SO_4^{-\cdot}$ was the predominant free radical under acidic conditions. When the pH was alkaline, part of $SO_4^{-\cdot}$ was prone to react to generate ·OH. Since its half-life in aqueous solution was shorter than that of $SO_4^{-\cdot}$, it may lead to insufficient contact time between ·OH and RB5, thus reducing the degradation rate [35]. Given that the initial pH value of RB5 wastewater was around 6, a suitable pH value of 6 was determined through comprehensive consideration and will be used for subsequent research.

3.4 Stability Analysis

Figure 9 showed the reproducibility of the degradation performance results of the Fe-GO/PDS system under the optimal reaction conditions. Analysis revealed that after repeating the operation five times, the removal effect of RB5 remained basically constant, with the removal rate exceeding 90% after a reaction time of 180 min. This indicated that the removal effect of Fe-GO used to activate PDS for degrading RB5 in

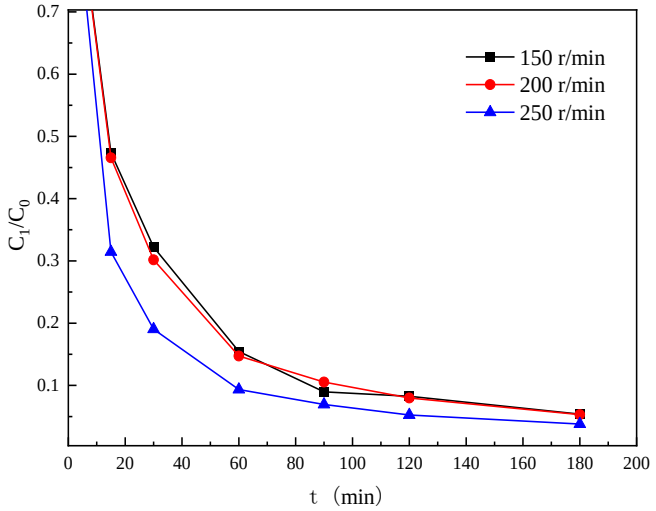

Figure 6. Influence of oscillation frequency on RB5 removal efficiency (conditions: [Fe-GO] = 0.08 g, [PDS] = 3 mmol/L, T = 25 ℃, v = 200 r/min, $pH_0 \approx 6$, [RB5] = 50 mg/L, and t = 180 min.)

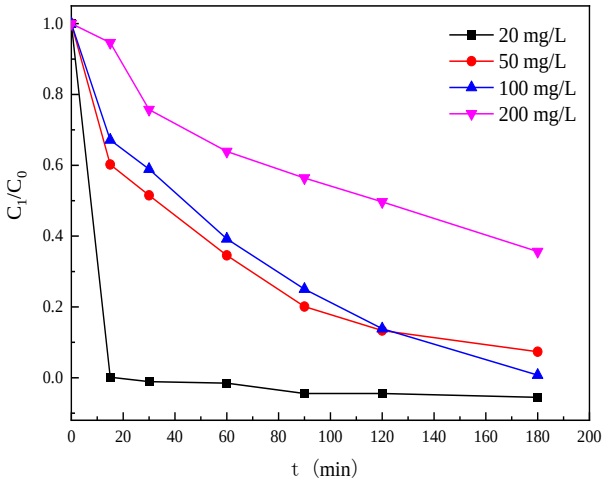

Figure 7. Effect of initial concentration on RB5 removal efficiency (conditions: [Fe-GO] = 0.08 g, [PDS] = 3 mmol/L, T = 25 ℃, v = 200 r/min, [RB5] = 50 mg/L, and t = 180 min)

simulated dye wastewater was stable, providing a theoretical basis for its practical application.

3.5 Ultraviolet-visible Spectral Analysis

For the Fe-GO/PDS activation system, the removal of RB5 may, on the one hand, be due to the fact that the free radicals generated in the system disrupt the chromogenic group -N=N- of RB5, that is, the molecular structure of RB5 changes and thus undergoes decolorization. On the other hand, it may be the result of the complete oxidation of RB5 into small molecules such as CO_2 and H_2O for direct removal. However, for the Fe-GO adsorption system, the removal of RB5 may be the consequence of the adsorption effect of Fe-GO. By performing a scan within the range of 190 - 800 nm using an ultraviolet-visible spectrophotometer to observe whether new absorption peaks are generated, the degradation pathway can be preliminarily inferred. Figure 10 showed the full-spectrum scans of the solutions treated by the Fe-GO/PDS activation system and the Fe-GO adsorption system. Analysis of Figure 10(a) revealed that with the increase in reaction time, the absorbance values of the naphthalene ring structure of RB5 at 310 nm and the azo structure representing the chromogenic group at 600 nm gradually decreased [36]. After a reaction time of 180 min, the removal rate of RB5 in the Fe-GO/PDS system could reach up to 99%, and a new absorption peak seemed to be generated at 210 nm. However, the TOC removal rate was 92.9%. Compared with Figure 10(b), it could be seen that the characteristic peaks of RB5 decreased synchronously with the prolongation of time during the reaction process. Comprehensive analysis infers that most of RB5 is decolorized and finally removed through redox reactions such as those involving free radicals and active [H], while a small part remains in the wastewater in the form of intermediate products.

3.6 Quenching Experiment

Different amounts of tertiary butyl alcohol (TBA) and methanol were added to the reaction system to identify ·OH and SO_4^{-}· in the reaction system [37], and p-benzoquinone and L-histidine were used as quenchers to quench O_2^{-}· and $^1O_2$ in the reaction system, respectively [38]. Figure 11 illustrated the inhibitory effect of quenchers on the removal efficiency of RB5 by the Fe-GO/PDS system. As could be seen from Figure 11(a), methanol and tert-butanol exerted significant inhibitory effects on the removal efficiency of RB5, preliminarily suggesting the existence of SO_4^{-}· and ·OH in the Fe-GO/PDS activation system. However, perhaps due to the fact that Fe-GO contained numerous micropores and mesopores whose surfaces could bind SO_4^{-}· and ·OH [21], it was impossible to achieve effective quenching with methanol. From Figure 11(b), it was evident that in the presence of p-benzoquinone and L-histidine, the removal of RB5 was inhibited to varying degrees, indicating the existence of O_2^{-}· and $^1O_2$ in the Fe-GO/PDS system. Among them, the inhibitory effect of L-histidine was prominent, implying that $^1O_2$ played a crucial role in the removal process of RB5. Nevertheless, the existence of SO_4^{-}·, ·OH, O_2^{-}· and $^1O_2$ required further identification by EPR.

4. Conclusion

In this paper, Fe_3O_4/graphene oxide composite (Fe-GO) was prepared via the hydrothermal method, and the successful preparation of Fe-GO was confirmed by means of XRD, SEM, EDS, and VSM characterizations. The

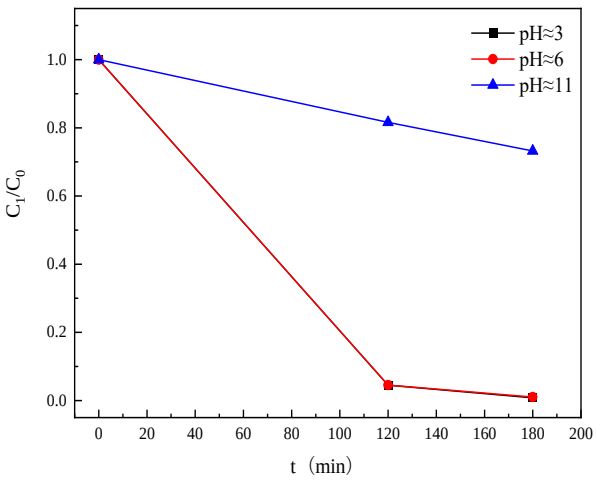

Figure 8. Effect of initial pH value on RB5 removal efficiency (conditions: [Fe-GO] = 0.08 g, [PDS] = 1 mmol/L, T = 25 ℃, v= 200 r/min, pH ≈ 6, and t = 180 min.

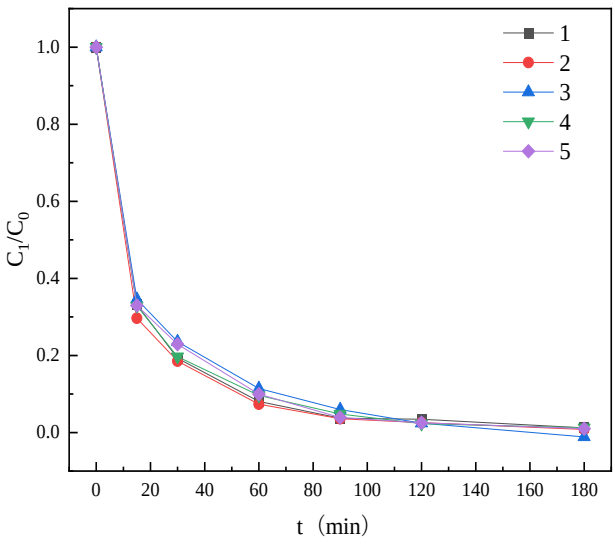

Figure 9. Stability of RB5 degradation by Fe-GO activated PDS.

results demonstrated that under the conditions of a Fe-GO dosage of 0.8 g/L, a PDS dosage of 3 mol/L, a stirring speed of 200 r/min, pH ≈ 6, and at 25 °C, the removal rate of RB5 could reach 99.2% with excellent reproducibility, indicating that the method was stable and feasible. Fe-GO exhibits good dispersibility, enhanced thermal stability, and strengthened magnetism, allowing for the direct recovery of Fe-GO by applying an external magnetic field. Overall, compared with GO, the activation and adsorption capabilities of magnetically modified Fe-GO have both been improved. The degradation of RB5 in the Fe-GO/PDS degradation system is the result of the combined effects of Fe-GO adsorption and activation. Part of the RB5 molecules are removed due to the adsorption effect of Fe-GO, while on the other hand, Fe^{2+}, GO activates PDS to generate free radicals such as SO_4^{-}, ·OH, O_2^{-}· and $^1O_2$, which oxidize RB5 for removal, among which $^1O_2$ plays a crucial role in the removal process of RB5.

Acknowledgement

This research was financially Liaoning Key Laboratory of Chemical Additive Synthesis and Separation Project (ZJNK2014, ZJNK2420).

CRediT Author Statement

Author Contributions: Z.S. contributed to the investigation, writing—original draft, reviewing, and methodology. W.Z. contributed to data processing and drawing. J.W contributed to the writing—original draft. Z.L. contributed to analysis SEM. K.S. contributed to language modification. W.K. contributed to reviewing. All authors have read and agreed to the published version of the manuscript.

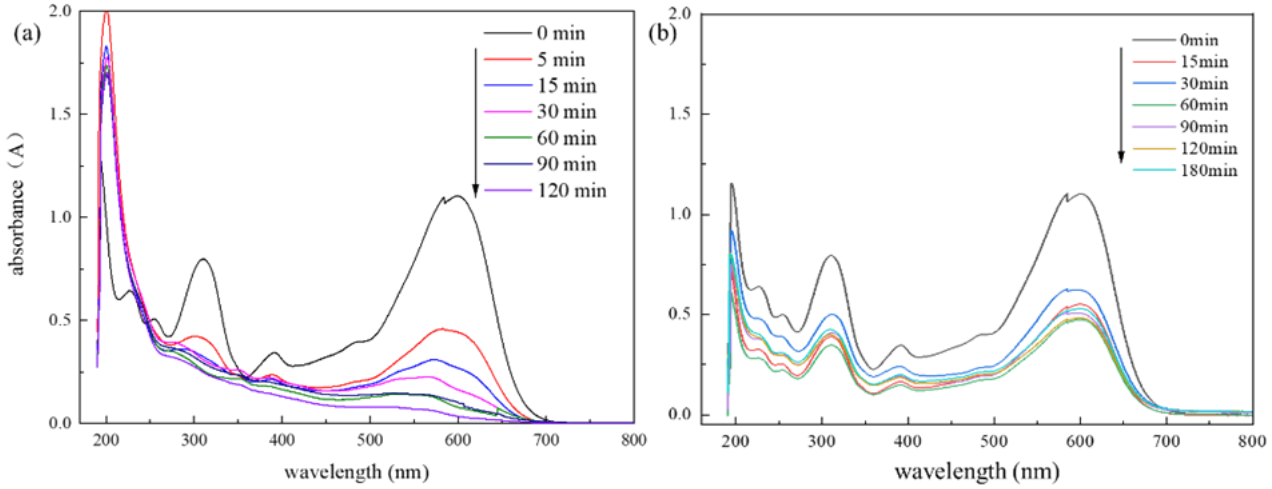

Figure 10. Full spectrum scanning diagram of UV-Vis spectrophotometer: (a) Fe-GO/PDS activation system (b) Fe-GO adsorption system.

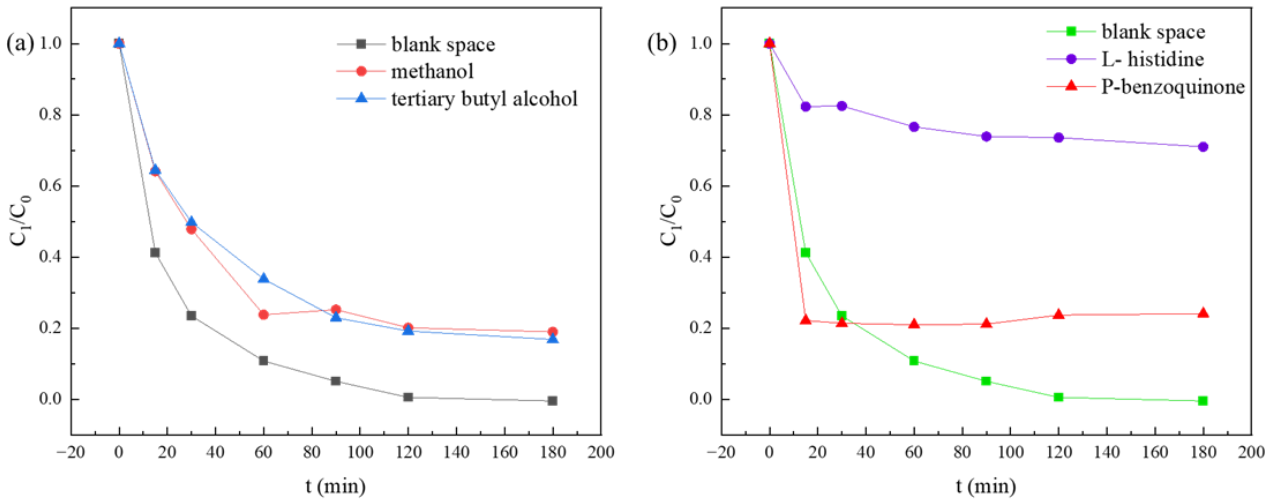

Figure 11. Effect of quencher on degradation of RB5 in Fe-GO/PDS system: (a) methanol and tert-butanol (b) L- histidine and p-benzoquinone.

References

[1] Alves de Lima, R.O., Bazo, A.P. (2007) Favero Salvadori D M, et al. Mutagenic and carcinogenic potential of a textile azo dye processing plant effluent that impacts a drinking water source. *Mutation Research-Genetic Toxicology and Environmental Mutagenesis*, 626 (1-2), 53-60. DOI: 10.1016/j.mrgentox.2006.08.002.

[2] Khan, S., Malik, A. (2018) Toxicity evaluation of textile effluents and role of native soil bacterium in biodegradation of a textile dye. *Environ. Sci. Pollut. R.*, 25(5), 4446-4458. DOI: 10.1007/s11356-017-0783-7.

[3] Lu, J., Zhou, Y., Lei, J., Ao, Z., Zhou. Y. (2020) Fe_3O_4/graphene aerogels: A stable and efficient persulfate activator for the rapid degradation of malachite green. *Chemosphere*, 251, 126402-126413. DOI: 10.1016/j.chemosphere.2020.126402.

[4] Zhou, Y., Lu, J., Zhou, Y., Liu, Y. (2019) Recent advances for dyes removal using novel adsorbents: A review. *Environmental Pollution*, 252, 352-365. DOI: 10.1016/j.envpol.2019.05.072

[5] Ghaffar, A., Mehdi, M., Otho, A.A., Tagar, U., Hakro, R.A., Hussain, S. (2023) Electrospun silk nanofibers for numerous adsorption-desorption cycles on Reactive Black 5 and reuse dye for textile coloration. *Journal of Environmental Chemical Engineering*, 11(6), 111188-111197. DOI: 10.1016/j.jece.2023.111188.

[6] Vinayak, A., Singh, G.B. (2022) Biodecolorization of reactive black 5 using magnetite nanoparticles coated Bacillus sp. RA5. Materials Today: *Proceedings*, 48, 1523-1526. DOI: 10.1016/j.matpr.2021.09.425.

[7] Cao, Y., Liu, W., Qian, J., Cao, T., Wang, J., Qin, W. (2019) Porous Organic Polymers Containing a Sulfur Skeleton for Visible Light Degradation of Organic Dyes. *Chemistry-an Asian Journal*, 14 (16), 2883-2888. DOI: 10.1002/asia.201900477.

[8] Li, M.F., Liu, Y.G., Zeng, G.M., Liu, N., Liu, S.B. (2019) Graphene and graphene-based nanocomposites used for antibiotics removal in water treatment: A review. *Chemosphere*, 226, 360-380. DOI: 10.1016/j.chemosphere.2019.03.117.

[9] Luo, L.X., Zhang, M.J., Wang, B., Mei, L.Y., Li, B.H. (2019) Gra Pilot-scale Application Test of Low-intensity Ultrasonic-enhanced Coagulation Technology. *Industrial Safety and Environmental Protection*, 45(01), 12-14. (in chinese).

[10] Vijayaraghavan, K., Yun, Y.-S. (2007) Utilization of fermentation waste (Corynebacterium glutamicum) for biosorption of Reactive Black 5 from aqueous solution. *J. Hazard. Mater.*, 141(1), 45-52. DOI: 10.1016/j.jhazmat.2006.06.081.

[11] Ma, L. (2022) Study on the Treatment of Azo Dye Wastewater by CoMnFe-Hydrotalcite/Graphene Activated Persulfate. *Anshan: University of Science and Technology Liaoning*, 2022. (in chinese)

[12] Kou, Q.Q. (2022) Research on the Degradation of Dye Wastewater by Iron-Manganese Oxide Composite Carbon Nanotubes Activated Persulfate. *Chongqing: Chongqing University*, 2022. (in chinese)

[13] Mohod, A.V., Momotko, M., Shah, N.S., Marchel, M., Imran, M., Kong, L., Boczkaj, G. (2023) Degradation of Rhodamine dyes by Advanced Oxidation Processes (AOPs) – Focus on cavitation and photocatalysis - A critical review. *Water Resources and Industry*, 30, 100220-100249. DOI: 10.1016/j.wri.2023.100220.

[14] Zhou, B., Wang, J.J., Dangal, P., Lomnicki, S., Roy, A.D., Park, J.H. (2024) A novel sugarcane residue-derived bimetallic Fe/Mn-biochar composite for activation of peroxymonosulfate in advanced oxidation process removal of azo dye: Degradation behavior and mechanism. *Journal of Water Process Engineering*, 58, 104740-104754. DOI: 10.1016/j.jwpe.2023.104740.

[15] Sun, Y., Zhao, J., Zhang, B.-T., Li, J., Shi, Y., Zhang, Y. (2019) Oxidative degradation of chloroxylenol in aqueous solution by thermally activated persulfate: Kinetics, mechanisms and toxicities. *Chem. Eng. J.*, 368, 553-563. DOI: 10.1016/j.cej.2019.02.208.

[16] Wu, .J, Wang, B., Cagnetta, G., Huang, J., Wang, Y., Deng, S., Yu, G. (2020) (Nanoscale zero valent iron-activated persulfate coupled with Fenton oxidation process for typical pharmaceuticals and personal care products degradation. *Separation and Purification Technology*, 239, 116534-116542. DOI: 10.1016/j.seppur.2020.116534.

[17] Wu, G., Kong, W., Gao, Y., Kong, Y., Dai, Z., Dan, H., Shang, Y., Wang, S., Yin, F., Yue, Q., Gao, B. (2022) Removal of chloramphenicol by sulfide-modified nanoscale zero-valent iron activated persulfate: Performance, salt resistance, and reaction mechanisms. *Chemosphere*, 286, 131876-131887. DOI: 10.1016/j.chemosphere.2021.131876.

[18] Zubir, N.A., Yacou C., Motuzas, J., Zhang, X., Diniz da Costa, J.C. (2014) Structural and functional investigation of graphene oxide–Fe_3O_4 nanocomposites for the heterogeneous Fenton-like reaction. *Scientific Reports*, 4(1), 4594. DOI: 10.1038/srep04594.

[19] Song, M., Nguyen, Q.B., Kim, C., Hwang, I. (2023) Sustained activation of persulfate by slow release of Fe(II) from silica-coated nanosized zero-valent iron for in situ chemical oxidation. *Water Res.*, 246, 120715-120725. DOI: 10.1016/j.watres.2023.120715.

[20] Park, C.M., Heo, J., Wang, D., Su, C., Yoon, Y. (2018) Heterogeneous activation of persulfate by reduced graphene oxide-elemental silver/magnetite nanohybrids for the oxidative degradation of pharmaceuticals and endocrine disrupting compounds in water. *Applied Catalysis B Environmental An International Journal Devoted to Catalytic Science & Its Applications*, 225, 91-99. DOI: 10.1016/j.apcatb.2017.11.058.

[21] Fu, H., Zhao, P., Xu, S., Cheng, G., Li, Z., Li, Y., Li, K., Ma, S. (2019) Fabrication of Fe_3O_4 and graphitized porous biochar composites for activating peroxymonosulfate to degrade p-hydroxybenzoic acid: Insights on the mechanism. *Chem. Eng. J.*, 375, 121980-121993. DOI: 10.1016/j.cej.2019.121980.

[22] Yu, Y., Guo, H., Zhong, Z., Wang, A., Xiang, M., Xu, S., Dong, C., Chang, Z. (2022) Fe_3O_4 loaded on ball milling biochar enhanced bisphenol a removal by activating persulfate: Performance and activating mechanism. *J. Environ. Manage.*, 319, 115661-115672. DOI: 10.1016/j.jenvman.2022.115661.

[23] Dolatabadi, M., Świergosz, T., Wang, C., Ahmadzadeh, S. (2023) Accelerated degradation of groundwater-containing malathion using persulfate activated magnetic Fe3O4/graphene oxide nanocomposite for advanced water treatment. *Arabian Journal of Chemistry*, 16(1), 104424-104437. DOI: 10.1016/j.arabjc.2022.104424.

[24] Dibaji, Y., Zilouei, H., Bazarganipour, M. (2023) Removal of MTBE from aqueous solution using reduced graphene oxide/Fe_3O_4 nanocomposite. *Environmental Nanotechnology, Monitoring & Management*, 20, 100842-100853. DOI: 10.1016/j.enmm.2023.100842.

[25] Wang, S., Wang, J. (2024) Ionizing radiation-assisted in-situ synthesis of nitrogen-doped graphene oxide-supported nano Fe_3O_4 for PMS activation to degrade emerging pollutants. *Radiation Physics and Chemistry*, 214, 111312-111318. DOI: 10.1016/j.radphyschem.2023.111312.

[26] Peng, S.-Y., Lin, Y.-W., Lin, Y.-Y., Lin, K.L. (2024) Hydrothermal synthesis of hydroxyapatite nanocrystals from calcium-rich limestone sludge waste: Preparation, characterization, and application for Pb^{2+} adsorption in aqueous solution. *Inorganic Chemistry Communications*, 160, 111943-111956. DOI: 10.1016/j.inoche.2023.111943.

[27] Feng, P., Zhao, R., Yang, L., Chen, S., Wang, D., Pan, H., Shuai, C. (2022) Hydrothermal synthesis of hydroxyapatite nanorods and their use in PCL bone scaffold. *Ceramics International*, 48(22), 33682-33692. DOI: 10.1016/j.ceramint.2022.07.314.

[28] Zhu, X., Zhang, B., Ye, Z., Shi, H., Shen, Y., Li, G. (2015) An ATP-responsive smart gate fabricated with a graphene oxide-aptamer-nanochannel architecture. *Chem. Commun.*, 51(4), 640-643. DOI: 10.1039/c4cc07990f.

[29] Vuong Hoan, N.T., Anh Thu, N.T., Duc, H.V., Cuong, N.D., Quang Khieu, D., Vo, V. (2016) Fe_3O_4/Reduced Graphene Oxide Nanocomposite: Synthesis and Its Application for Toxic Metal Ion Removal. *Journal of Chemistry*, 2016, 1-10. DOI: 10.1155/2016/2418172.

[30] Li, L., Shi, K., Xiong, S., Zhang, S., Shan, Z., Qian, G., Zhai, X., Xiao, P., Narayanasamy, S. (2023) Study on Phosphorus Adsorption Performance of Inorganic Modified Green Mudstone. *Adsorpt. Sci. Technol.*, 2023, 1-14. DOI: 10.1155/2023/3574652.

[31] Xiao, S., Zhang, L., Zhou, L., Zhong, H., Brusseau, M.L., Li, Y., Wang, Y., Liu, G., Zhang, J. (2024) The long-term effect of Fe_3O_4 in activating persulfate to degrade refractory organic contaminants for groundwater remediation. *Chem. Eng. J.,* 482, 148801-148813. DOI: 10.1016/j.cej.2024.148801.

[32] Zhang, W.Q. (2024) Research on the Degradation of Bisphenol A in Water by Activated Carbon-supported Iron-manganese Oxides Activated Persulfate. *Nanchang: Nanchang University*. (in chinese)

[33] Liu, J., Zhao, Z., Shao, P., Cui, F. (2015) Activation of peroxymonosulfate with magnetic Fe_3O_4–MnO_2 core–shell nanocomposites for 4-chlorophenol degradation. *Chem. Eng. J.*, 262, 854-861. DOI: 10.1016/j.cej.2014.10.043.

[34] Xu, Y., Dong, X., Chen, Y., Liu, N., Zhang, X., Song, C., Fan, X. (2024) Constructing 3D hierarchical Fe@RGO supported nitrogen-doped carbon nanotubes to enhance peroxymonosulfate activation for achieving efficient antibiotic degradation. *Colloids and Surfaces A: Physicochemical and Engineering Aspects*, 702, 135017-135029. DOI: 10.1016/j.colsurfa.2024.135017.

[35] Liu, L., Lin, S., Zhang, W., Farooq, U., Shen, G., Hu, S. (2018) Kinetic and mechanistic investigations of the degradation of sulfachloropyridazine in heat-activated persulfate oxidation process. *Chem. Eng. J.*, 346, 515-524, DOI: 10.1016/j.cej.2018.04.068.

[36] Cao, H.L. (2020) Research on the Preparation of Iron-based Composite Materials Based on Persulfate and the Efficiency of Removing Reactive Black 5. *Nanchang: Nanchang University*. (in chinese)

[37] Zeng, T., Zhang, X., Wang, S., Niu, H., Cai, Y. (2015) Spatial Confinement of a Co_3O_4 Catalyst in Hollow Metal–Organic Frameworks as a Nanoreactor for Improved Degradation of Organic Pollutants. *Environmental Science & Technology*, 49(4), 2350-2357. DOI: 10.1021/es505014z.

[38] Ma, W., Wang, N., Du, Y., Tong, T., Zhang, L., Andrew Lin, K.Y., Han, X. (2019) One-step synthesis of novel Fe_3C@nitrogen-doped carbon nanotubes/graphene nanosheets for catalytic degradation of Bisphenol A in the presence of peroxymonosulfate. *Chem. Eng. J.*, 356, 1022-1031. DOI: 10.1016/j.cej.2018.09.093.